Two-tissue Compartmental Modeling

A simplified two tissue compartmental model for ^{18}F-FDG is shown in Supplemental Figure 6, where $C_p(t)$, $C_1(t)$ and $C_2(t)$ are the time varying plasma, free and bound tracer activity concentrations (Bq/mL); $\mathrm{K}_1, \mathrm{k}_2, \mathrm{k}_3$ and k_4 are the kinetic rate constants which control the rate of tracer exchange between compartments. In order to simulate time–activity curves, an irreversible two tissue compartmental model (i.e., $\mathrm{k}_4 = 0$) was implemented. Additionally, the vascular fraction (F_b) was assumed to be zero. The equations for this model can be written in the following manner:

$$\frac{dC_1(t)}{dt} = \mathrm{K}_1 C_p(t) - \mathrm{k}_2 C_1(t) - \mathrm{k}_3 C_1(t)$$

$$\frac{dC_2(t)}{dt} = \mathrm{k}_3 C_1(t)$$

$$C_{model}(t) = C_1(t) + C_2(t).$$

Here, $C_{model}(t)$ is the observed activity concentration of the target tissue. The model parameters ($\mathrm{K}_1, \mathrm{k}_2$ and k_3) are estimated by solving the ordinary differential equations and minimizing a weighted least square objective function. The net influx rate (K_i) was computed as:

$$\mathrm{K}_\mathrm{i} = \frac{\mathrm{K}_1 * \mathrm{k}_3}{\mathrm{k}_2 + \mathrm{k}_3}.$$

Preclinical Experiments

Six-week-old Naval Medical Research Institute nu/nu mice (n = 4) were ordered from Charles River, Germany and allowed to acclimatize in the on-site animal vivarium before being subcutaneously injected with 4.5 × 10^6 Colo-205 tumor cells on the right hind leg. The tumor size as well as normal social activity of animals was monitored during the entire study. When the tumors were palpable and showed signs of vascularization with a minimum length of 5 mm, the imaging experiments were started. Before and during tumor inoculation and imaging experiments, mice spontaneously respired 1.5% isoflurane dissolved in 100% O_2 at a flow rate of 0.8 L/min in order to maintain a deep anesthesia. All experiments were carried out in a specific-pathogen-free environment.

Three line sources were placed on the animal holder in order to co-register PET and magnetic resonance imaging (MRI) data. The mice were placed with the tumor in the middle

of the field-of-view of the Inveon dedicated small animal PET scanner (Siemens, Knoxville, TN, USA) and 12.0 MBq of ^{18}F-FDG in 50 µL of 0.9% NaCl was injected in the tail vein at a flow rate of 0.5 mL/min using an automated syringe pump system (Harvard Apparatus, Hollistion, MA, USA) directly after starting the PET acquisition. Scans were acquired using manufacturer-supplied software (Inveon Acquisition Workplace, version number 1.5.0.28) for 60 min and reconstructed using OSEM3D/FastMAP (reconstruction software version: 2.5, histogram version: 2.39 and re-binning version: 2.5) with the following framing: {10×2 s, 4×5 s, 2×10 s, 3×1 min, 3×2 min, 5×10 min}. Other reconstruction parameters were as follows: image zoom = 1, image matrix size = 256×256×159 with (0.39×0.39×0.80) mm^3 voxel sizes, OSEM3D Iterations = 2, MAP Iterations = 18, Beta = 0.05, Uniform set to Resolution and FastMAP setting on.

After the PET scans, the animal holder was moved to a 7 T Clinscan (Bruker BioScan, Ettlingen, Germany) small animal MRI while maintaining the position of the mouse. The following settings were used for the T2 weighted turbo spin echo sequence (T2tse): repetition time (TR) = 3000 ms, echo time (TE) = 205 ms, echo train length = 161, image size = 256×160 and voxel size (mm^3) = 0.22×0.22×0.22.

PET images were co-registered to MR images using a marker-based, semi-automatic co-registration tool in PMOD 3.2 (PMOD Technologies, Zurich, Switzerland) and the T2tse images were used as an anatomical reference for drawing volumes of interest (VOIs) on each tumor. Special care was taken to exclude the skin of the mice during the VOI placement on the tumors in T2tse images. The voxel values along with the coordinates from each VOI for all PET and MRI measurements were exported and further processed in MATLAB (Mathworks, Natick, MA, USA).

Histology

The histology and immunohistochemistry of one tumor was obtained to validate the results of SC on ^{18}F-FDG measurements. Following the dynamic PET scan, the mouse was sacrificed and a line was drawn on the tumor parallel to the transversal imaging plane. The tumor was removed using a scalpel and sectioned into two halves along the aforementioned line. The individual halves were kept in neutral buffered formaldehyde (4.7% by volume) and embedded into paraffin, before processing for staining. For histology, 3-5 µm-thick sections were cut and stained with haematoxylin and eosin. Immunohistochemical stainings with an anti-CD31 antibody (Abcam plc) were performed on an automated immunostainer (Ventana Medical Systems, Inc.) according to the company's protocols with slight modifications. Appropriate positive and negative controls were used to confirm the adequacy of the staining. Only a rigid co-registration was performed between the histology and imaging data.

The matching imaging slice was selected based on the visual alignment of the contours of the PET and histology image.

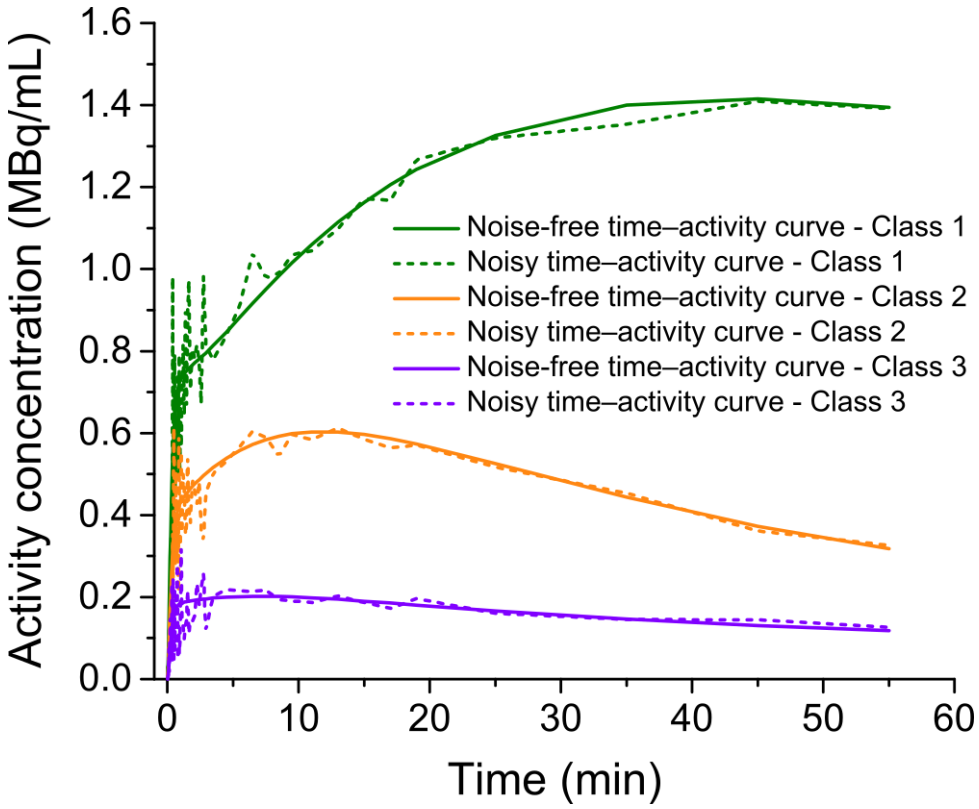

Supplemental figure 1. Preclinical noise-free and noisy (for ß = 0.5) time–activity curve samples of class 1, class 2, and class 3.

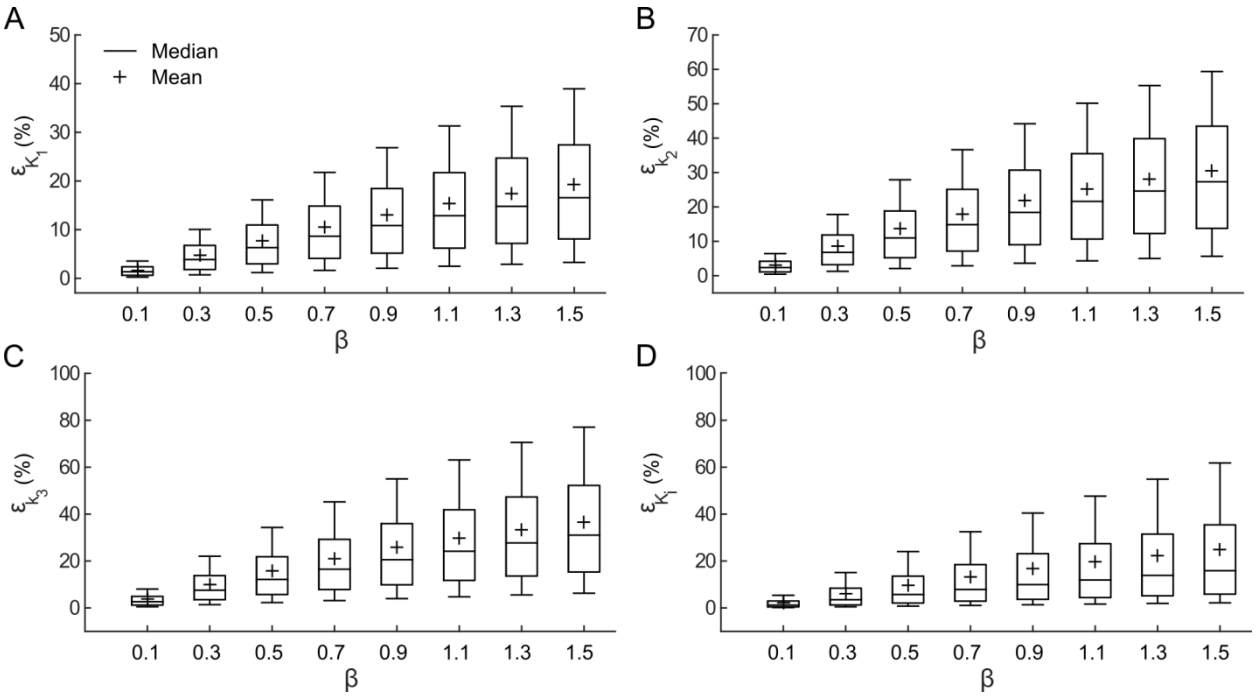

Supplemental figure 2. Absolute ε for clinical simulations with an increase in the amount of noise (ß) for K_1 (A), k_2 (B), k_3 (C), and K_i (D). The boxes depict the interquartile range and whiskers represent the 10th and 90th percentiles of the data.

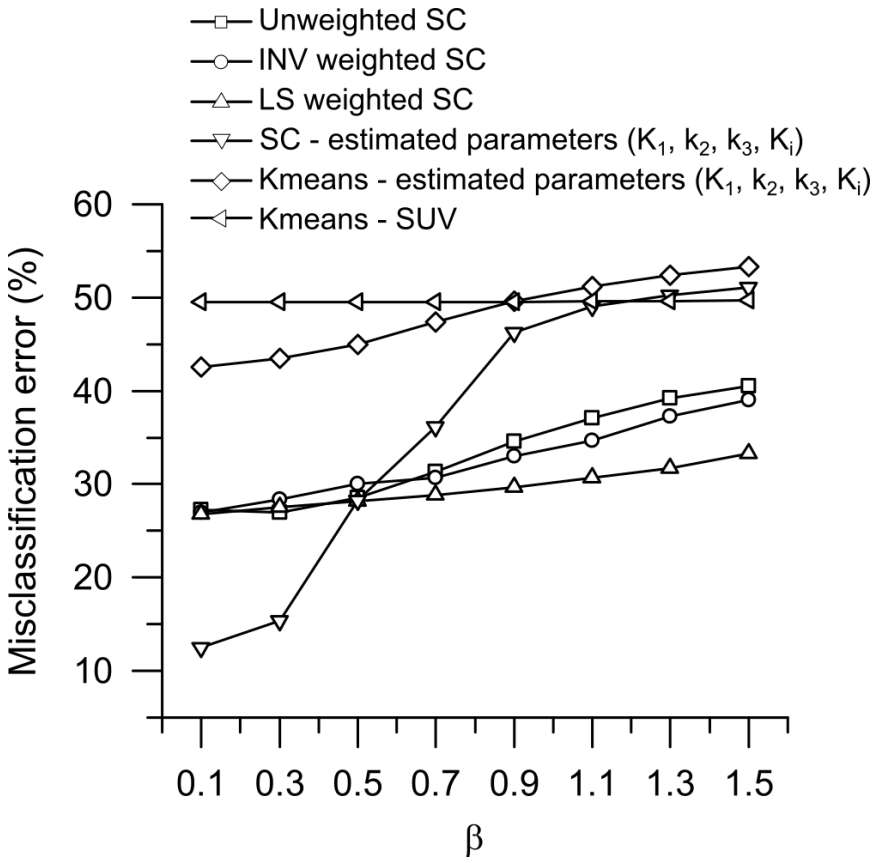

Supplemental figure 3. Misclassification error of various clustering schemes for clinical simulations with an increase in the amount of noise (ß).

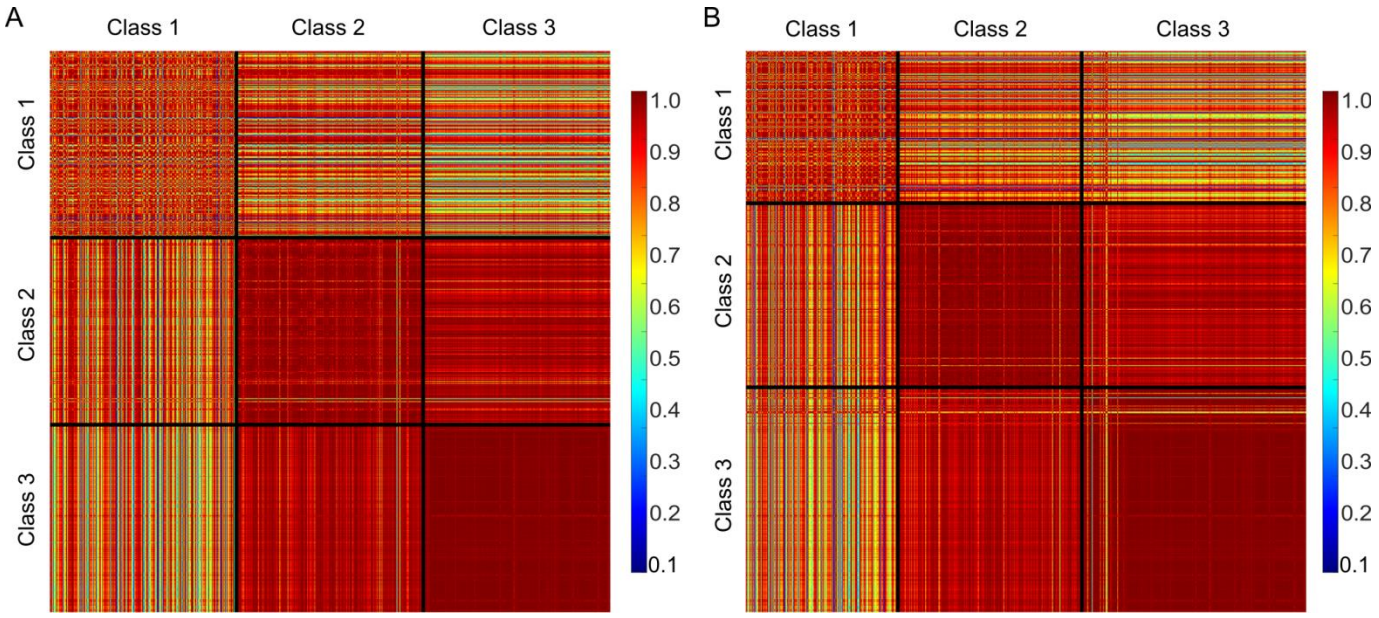

Supplemental figure 4. Ground truth (A) and clustering (B) affinity matrices of the preclinical noise-free time–activity curves (shown in Fig. 1B). The three block diagonal matrices (top to bottom) depict the intra-class similarity of class 1, 2, and 3. The rest of the two off-diagonal block matrices in each row display the inter-class similarity between the annotated classes. As the time–activity curves of class 2 and class 3 were relatively similar in shape (Fig. 1B), the inter-class similarity between these two clusters was also higher. On the other hand, despite significant overlap, the inter-class similarity between class 1 and class 2 was relatively lower, primarily due the differences in the shape of the simulated time–activity curves.

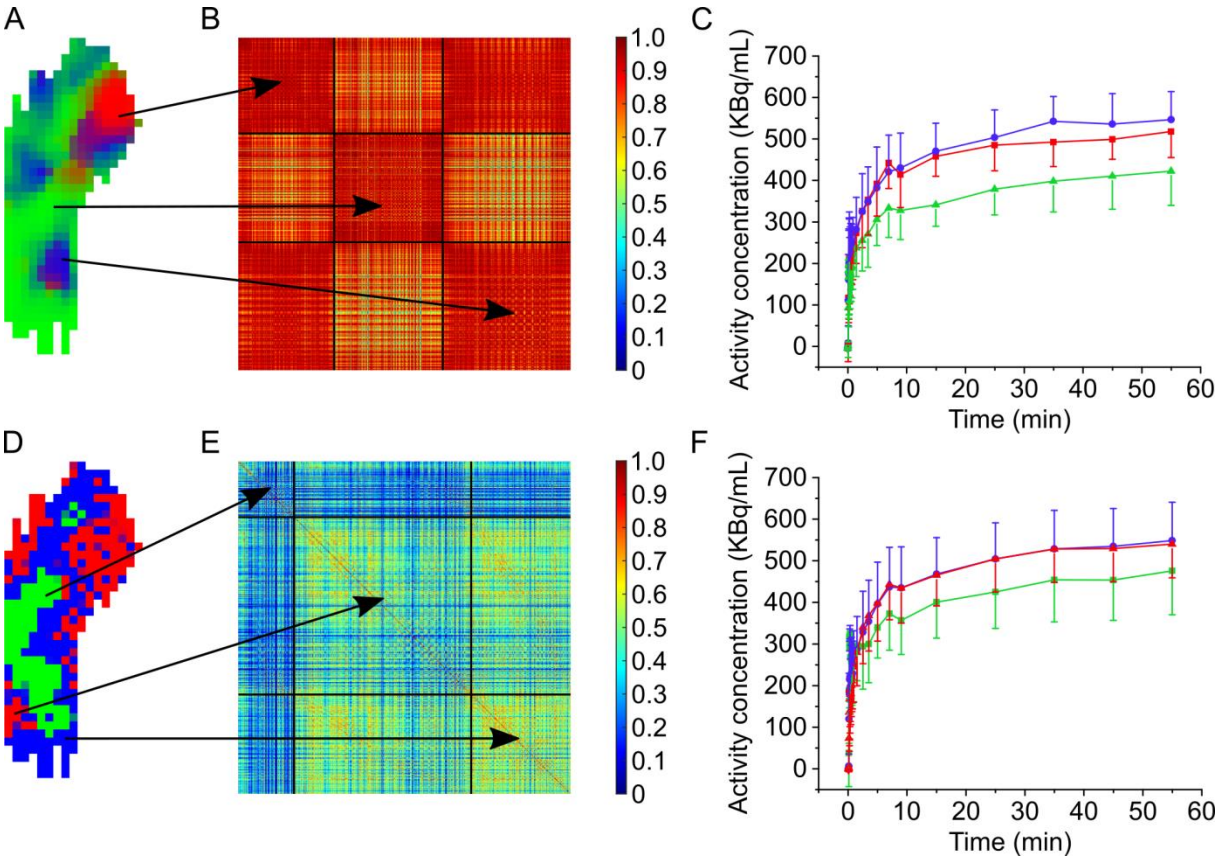

Supplemental figure 5. (A) SC segmented image of a representative tumor with three clusters obtained using dynamic ^{18}F-FDG PET data. (B) Affinity matrix of the entire tumor volume computed using the clustering solution in A. The comparable cluster population of the green and blue regions is due to the fact that the end slices of the tumor are densely vascularized in contrast to the center ones. (C) Averaged time–activity curves of the respective clusters. While all three clusters depict high intra-class similarity, the red and blue clusters also contain high inter-class similarity. As the red cluster appears on the periphery of the blue cluster, both the regions also have similar average time–activity curves. (D) Segmentation of the same tumor using the parametric maps (shown in Fig. 5) and SC. (E) Affinity matrix of the entire tumor volume computed using the clustering solution in D and PET time–activity curves. (F) Averaged time–activity curves of the respective clusters.

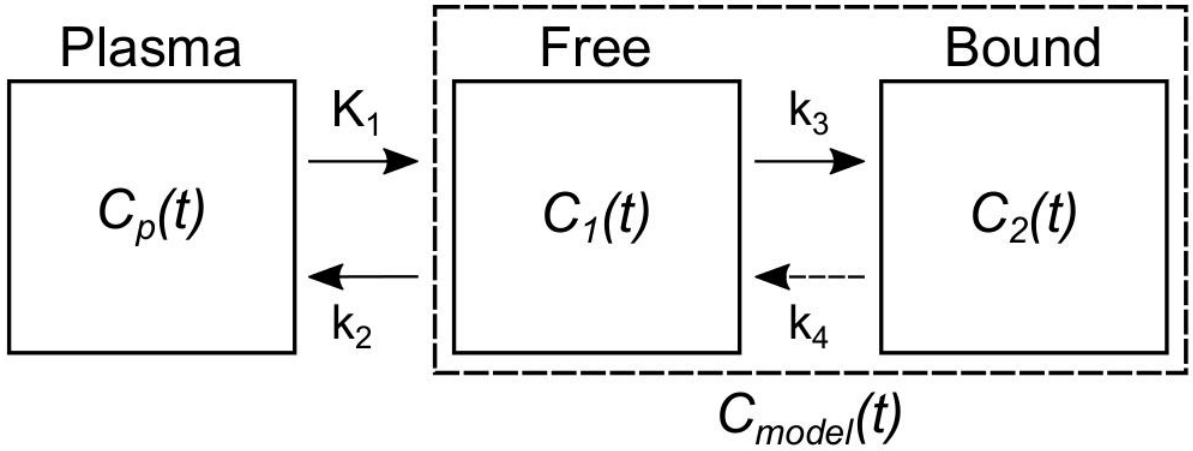

Supplemental figure 6. A two tissue compartmental model for ^{18}F-FDG PET. The dashed box represents the observed activity concentration of the region.